Dry Metal Forming Open Access Journal

Fast Manuscript Track

Edited by Frank Vollertsen
Available online at elib.suub.uni-bremen.de

www.drymetalforming.de

Dry Met. Forming OAJ FMT 1 (2015) 72–78
Received 5 February 2015; published 10 February 2015

# Selective oxidation of 1.2379 tool steel surfaces – an approach for Dry Metal Forming

Daniel Wulff*[1], Deniz Yilkiran[2], Ulrich Holländer[1], Dirk Lützenkirchen-Hecht[3], Ralph Wagner[3], Sven Hübner[2], Kai Möhwald[1], Hans Jürgen Maier[1], Bernd-Arno Behrens[2]

[1]Institut für Werkstoffkunde (Material Science), Leibniz Universität Hannover, An der Universität 2, 30823 Garbsen, Germany
[2]Institut für Umformtechnik und Umformmaschinen, Leibniz Universität Hannover, An der Universität 2, 30823 Garbsen, Germany
[3]Fachbereich C - Physik, Bergische Universität Wuppertal, Gaußstr. 20, 42097 Wuppertal, Germany

## Abstract

Subject of this work is the development of a simple and cost-efficient process for conditioning the surface of forming tools for deep drawing processes in order to minimize friction and wear to a level that dry forming processes without any lubricants will be possible in future. The approach chosen is an oxidative heat treatment of the tool surfaces at controlled oxygen partial pressures and temperatures. Thus, alloying elements of the tool shall constitute oxide layers with advantageous tribological properties suitable for the aimed application. In this paper results from parameter studies concerning the controlled surface oxidation of a hardened conventional tool steel (EU alloy grade 1.2379 X153CrMoV12) are presented. Beside the dependence of the oxide layer morphology from the chosen heat treatment parameters first results of their tribological behavior gained from measurements of the friction coefficients using an application-oriented strip drawing test are presented. From these investigations promising results and conclusions for future work have been obtained which are discussed in the paper.

**Keywords:** strip drawing test, friction, SEM, GIXRD, surface layer

## 1 Introduction

The profitable production in the modern industrial manufacturing requires a maximum life of the used tools. To make this possible the tribological relationships of the systems need to be analysed and understood. In particular, friction and wear are very important processes in relation to the tool life. According to current estimates it can be assumed that the direct losses in industrialised countries due to friction and wear are up to 7 % of the gross national product. Consequently only in Germany a total loss of about 35 billion euros per year occurs [1, 2]. In addition, there are further indirect losses due to e.g. production failures, maintenance costs as well as poor product quality requiring rework.

Forming technology represents a production industry that requires high volumes for profitability. Due to the forming process the tools are subject to high dynamic load changes. This is why they need to be protected against wear. In the field of sheet metal forming, the tribological stress of the tools is particularly high because the deformation zones often extend over the entire tool. There are great efforts to protect the tools against wear. Forming tools are generally hardened by heat treatments, so they have an increased wear resistance. Furthermore, in sheet metal forming, such as in deep drawing processes, the blanks are lubricated before forming. Thereby the resulting friction coefficient μ is reduced and the tools are cooled, too. Through the use of lubricants the tool life is increased as adhesive wear is avoided [2, 3]. Even the punch edge wear, which particularly occurs while cutting higher and highly resistant materials, can be decreased by reducing the coefficient of friction by the use of suitable lubricants [3].

Besides the advantages there are still disadvantages by the use of lubricants in sheet metal forming. The disposal is elaborate, costly and polluting. Another problem is the contamination of the stamping plants and the extension of the process chain requiring additional cleaning stations. For example, in the automotive industry residual oil particles on the component surfaces have a negative influence on the joining processes after forming. The residues are also contaminating the baths of


*E-mail address of corresponding author: d.wulff@iw.uni-hannover.de

cathodic dip coating [4, 5]. Accordingly the renunciation of lubricating oils can shorten the process chain, reduce the costs and realize a sustainable production process. By the requirement of constant part qualities and similar lifetime of the forming tools, solutions that reduce the use of lubricating oils have to be found. At the Institute of Forming Technology and Machines (IFUM) studies were carried out in the past, which dealt with sheet metal forming without the use of oils. In the research project tools and sheet metals were coated with friction reducing PVD coatings. This enabled a successful reduction of the friction coefficient. The high costs of the PVD coating, however, are in contrast to an economic solution for the dry forming [6].

An actual Priority Programme (SPP 1676) by the German Research Foundation (DFG) deals with modern approaches to reduce the use of lubricants in forming technology [7]. The subprojects of the SPP 1676 are focusing on solutions in the field of sheet metal forming as well as in the field of bulk metal forming.

In the following, results of one subproject of the SPP 1676 will be presented. The project deals with the development of a new friction reducing tool coating for sheet metal forming tools on the basis of metal-oxides, generated from alloy elements of the tool steel itself. The oxide layers are produced by heat treatments under controlled atmospheres on specimens made of hardened tool steel (EU alloy grade 1.2379 X153CrMoV12). In the present paper, the first surface analysis of differently heat treated specimens, and results of strip drawing tests, done with selected specimens, will be presented. To determine the resulting friction between the specimen and the sheet material strip drawing tests were carried out in one experimental setup. Here, various oxide layer modifications were tested under varying surface pressures.

## 2 Basic considerations to the generation and analysis of oxide layers on FeCr-steels

The approach investigated here is to generate a coating on the surfaces of the tools via an oxidative heat treatment. Like other tool coatings the formed oxides shall reduce the friction, because in absence of a lubricant the friction between uncoated tools and the forming materials would increase rapidly and significant wear on the tool surface may take place. Alike the oxide layer should have a uniform composition and a good adhesion strength to the base metal. On the other hand the tool has to maintain its mechanical characteristics for example the hardness and the dimensions in order to ensure a direct use of the tool without mechanical or thermal post-processing steps after the oxidative heat treatment. Therefore the process temperature must be kept under the annealing temperature of the tool steel and there should be no fast temperature changes within the treatment.

During heat treatment in oxidising atmospheres different oxide modifications can appear on the steel surface and have to be considered. Depending on the specific conditions set during the treatment (e.g. gas compositions and pressures, temperatures, etc.) and the exact composition of the used steel, different oxidation reactions have been observed. Many studies deal with the effects of Fe and Cr oxidation at high temperature treatments above 500 °C [8, 9, 10, 11] and below 500 °C [11, 12].

In general, the base metal can react to four different oxides, namely hematite ($\alpha$-$Fe_2O_3$), maghemite ($\gamma$-$Fe_2O_3$), magnetite ($Fe_3O_4$) and wüstite (FeO), the latter is however unstable below 570 °C, since it decomposes to $\alpha$-$Fe_2O_3$ and $Fe_3O_4$ [13]. It is worth mentioning that chromium oxides are even more stable thermodynamically at elevated temperatures compared to those of iron and can also be formed on the surface, even though chromium is only present in the alloy in a minor concentration. Chromium also constitutes four oxides with different chromium valences: CrO, $CrO_2$, $CrO_3$ and $Cr_2O_3$.

Thus, many different oxides can be formed in principle during the heat treatment in oxygen containing process gases. Furthermore a number of mixed oxide compounds of chromium and iron like the spinel $FeCr_2O_4$ are known which have to be taken into account too, when generating oxidised surfaces of chromium containing steels. The chemical composition and the thickness of an originating layer depend on the chosen process parameters. Therefore, especially thick oxide coatings are often composed of distinctive layers with different oxide compositions [14].

A chance to control the formation and to make the process reproducible is to control the partial pressure of oxygen. The supply of oxygen is very relevant. At the elevated temperature of 500 °C, however, the formation of oxide layers on the steel is likely even for small oxygen partial pressures, and thus, the process conditions concerning its atmosphere as well as the temperature-time-regime have to be adjusted properly. Especially the addition of monosilane ($SiH_4$) as a reducing gas with limited water residues plays a key role and makes it possible to control the oxygen partial pressure and the oxygen activity, respectively, at a very low level.

$SiH_4$ is an extremely reactive gas with a high chemical affinity to oxygen. Doping inert gases with $SiH_4$ can result in a quantitative removal of all oxygen and water residues in the gas according to the reactions:

$$SiH_4 + 2O_2 \rightarrow SiO_2 + 2H_2O \quad (1)$$

$$SiH_4 + 2H_2O \rightarrow SiO_2 + 4H_2 \quad (2)$$

These reactions can be observed in principle by controlling the oxygen level in an inert gas with an oxygen sensor, when adding monosilane to it. Thermodynamic calculations show that the stoichiometric point for the first reaction is located at a partial pressure of about $10^{-9}$ mbar oxygen, while the second reaction lies at about $10^{-23}$ mbar. Both values can be calculated via thermodynamic modelling of the silane-doped inert gas presented in [15]. Measurements show that $SiH_4$ concentrations of a few 10 ppm are enough to ensure extremely low oxygen levels in the process atmosphere of a shielding gas furnace.

However, if the oxides are present in the form of very thin surface films only, the examination of the

layers and their composition is very difficult, since conventional metallographic analysis of coatings fail on this thickness scale. Surface sensitive methods compatible to the layer thickness are required in this case. In the past, the structure and the composition of oxide layers on metals and semiconductors as well as their formation and reduction behaviour have intensively been investigated by using X-ray photoelectron spectroscopy, Auger electron spectroscopy (XPS & AES), scanning electron microscopy techniques (see e.g. [16, 17, 18, 19, 20]) as well as synchrotron techniques (e.g. [21, 22, 23]).

In this context X-ray diffraction is a valuable technique to analyse the crystal structure of the specimens. Likewise to other X-ray methods, XRD is surface sensitive by using the total external reflection geometry [24]. For incidence angles below the critical angle of total reflection, the penetration depth of the X-rays (i.e. the depth where the X-ray field has decayed to 1/e of its original value) is only a few nm and the reflected beam only contains information about the near surface region of the specimen. Thus, grazing incidence X-ray diffraction (GIXRD) experiments are important for analytical surface investigations in a broad range of scientific fields [25, 26, 27].

For the present experiments SEM, GIXRD and strip drawing tests were used to elucidate the morphology, crystal structure, chemical composition and friction behaviour of steel surfaces after different heat treatments in an industrial continuous annealing furnace at 500 °C. More specifically detailed information about the influence of a partial pressure of oxygen controlled by the addition of monosilane ($SiH_4$) will be shown.

## 3 Experimental Details

For the experiments specimens (length 50 mm, width 49.7 ± 0.2 mm, height 20 mm) made of tool steel (EU alloy grade 1.2379 X153CrMoV12) with a nominal composition of 84.75 % Fe, 12.00 % Cr, 1.55 % C, 0.90 % V and 0.80 % Mo were used. They were manufactured according to the geometry shown in Fig. 1.

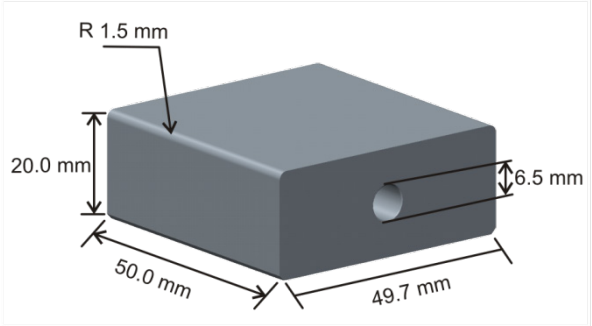


Fig. 1: Geometry of the specimen without deflection

The determination of the friction coefficients was performed at a temperature of 80 °C. For heating the specimens heating cartridges with a diameter of 6.5 mm and a length of 40 mm were placed in boreholes in the middle of the width-side. The temperature calibration was carried out by thermocouples type J, which was integrated into the heating cartridges. An additional alignment of the temperature was conducted on the surface of the specimen by a contact thermometer. The specimens were made of full metal and were then hardened. After the hardening, the surfaces were grinded with a belt sander to remove the black coverage that is a result of the hardening process to ensure reproducible starting conditions and a surface roughness of about $R_a = 0.6$ µm. Prior to the heat treatments, all specimens were cleaned in an ultrasonic bath with ethanol (96 %) for about 10 min. Afterwards they were first rinsed with pure acetone (> 99.5 %) and in a second step with pure ethanol (> 99.8 %). The specimens were wiped with precision paper towel after each step.

### 3.1 Thermal treatments with monosilane

The thermal treatments were performed in a conveyor belt furnace, which is especially equipped for experiments with monosilane-containing shielding gases [28]. The purities of the gases used were better than 99.996 %. By means of adding of $SiH_4$ to the inert carrier gas ($N_2$ or Ar) different partial pressures of oxygen were adjusted, covering an oxygen activity range between $10^{-5}$ and $10^{-23}$ within the furnace.

The necessary total amount of monosilane depends on the quality of the inert gas. The thermodynamic equilibrium conditions for the reaction of monosilane with oxygen and water result in a drastical drop of the oxygen activity between the two stochiometrical points, which make it impossible to adjust an exact partial pressure of oxygen between the first and the second stoichiometric point of the reaction. Therefore it is only possible to ensure a certain range for the partial pressure of oxygen and the oxygen activity, respectively, in which the specimens are exposed in the furnace.

Every thermal treatment in a conveyor belt furnace has a heat up, a holding and a cooling period. With respect to the high mass of the technical specimens the target temperature was reached after approximately 60 minutes with an accuracy of ±10 °C. After reaching the target temperature the specimens were hold in the heating zone for further 30 min and 60 min, respectively. For cooling the specimens were transferred into the cooling zone of the furnace and were kept there under process gas until the specimens reached room temperature again.

### 3.2 The principles of strip drawing tests

For the determination of the friction coefficients strip drawing tests with specimens without deflection were performed. This experimental setup represents the situation in the flange area of a deep drawing forming tool. The universal testing machine used for the strip drawing tests is shown in Fig. 2.

The testing machine can be used for different testing modes. In addition to the determination of the friction coefficient without deflection it is also possible to realise e.g. test setups with deflection or beads for the investigation of friction. The principle of the test setup without deflection is shown in the following Fig. 3.

During a test procedure two pistons are moved hydraulically in a vertical and a horizontal cylinder. On the vertical cylinder a sheet holder is mounted. In the experiment, the specimen is pressed due to the horizontal counter force $F_C$ to a sheet metal strip. Then the fixed strip is drawn upwards so that a vertical pulling force $F_P$

is resulting. To investigate only the friction between the specimen and the sheet metal strip, the sheet holder is supported by revolving bearings on the backside. The determination of the friction coefficient takes place via the recorded force relationships through Coulomb's law of friction as shown in the following equation 3.

$$F_R = \mu \cdot F_N \quad (3)$$

The normal force $F_N$ corresponds to the counter fore $F_C$ and the frictional force $F_R$ corresponds to the pulling force $F_P$ in the test setup.

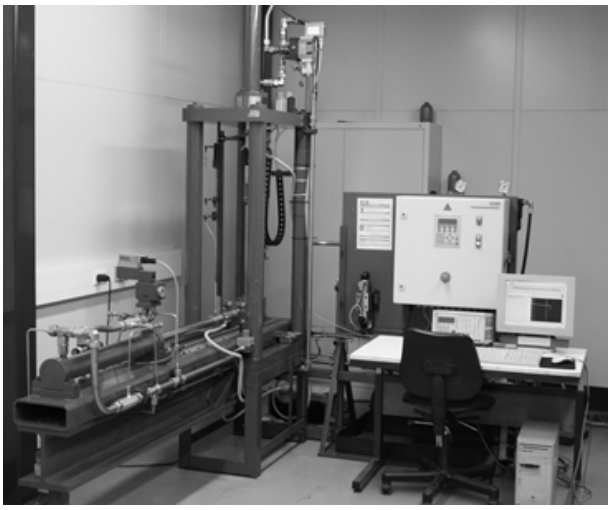

Fig. 2: Universal testing machine for the determination of friction coefficients

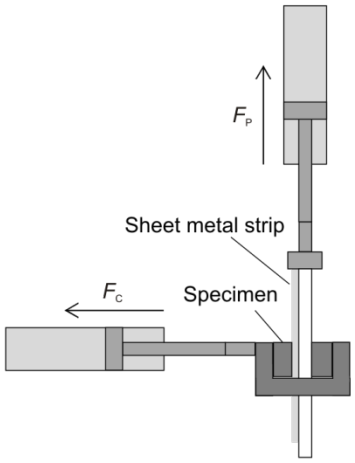


Fig. 3: Shematic representation of friction experiments without deflection

For the experiments, the sheet material DP600 + Z with a sheet thickness of 0.96 mm was used. The length of each strip was 700 mm and the width 20 mm. The sheet metal strips were cleaned with a 10 % solution of a cleaning composition (Tickopur R33). The friction coefficients were investigated for the contact pressure $P_N = 18$ N/mm$^2$. The choice of the surface pressure was based on real deep drawing data. Furthermore, the friction coefficients, as a result of the new coatings, should be determined at as high as possible contact pressures. The pulling velocity of all experiments was $v_P = 20$ mm/s and the temperature was constant at T = 80 °C. For statistical validation for each specimen 5 reruns were performed.

### 3.3 Surface analyses with SEM and GIXRD

The morphology of the specimen surfaces was observed by a high resolution scanning electron microscope (Zeiss Supra 55 VP) with secondary emission and in lens detector using an acceleration voltage of 7 kV. The crystallographic structure of the steel surfaces was investigated by grazing incidence X-ray diffraction (GIXRD) using synchrotron radiation from the DELTA storage ring (Dortmund, Germany) operating at an electron energy of 1.5 GeV, injection currents of 120 mA and about 10-12 h lifetime [29]. The experiments were performed at the wiggler beamline BL10, which is designed for X-ray absorption spectroscopy, diffraction measurements and surface sensitive X-ray reflectivity experiments in the energy range between approximately 4 keV and 16 keV. It employs a Si(111) channel-cut monochromator suited for high resolution X-ray experiments making use of the intense radiation emitted by a superconducting 5.3 T wiggler [30]. BL 10 is equipped with a 6-circle diffractometer to allow a precise alignment of the specimens within the X-ray beam, and a PILATUS 100K detector system (Dectris, Baden, Switzerland) for the diffraction experiments [31, 32].

All GIXRD measurements were performed at an energy of 10 keV and a threshold of 8.5 keV to eliminate the contributions of fluorescence radiation from the specimens to the recorded diffraction patterns. The incidence angles were varied between 1° and 6°, while the PILATUS detector was fixed at a diffraction angle of 45°, so that a Bragg angle of about 35° to 55° is covered by the experiments. The incident beam was collimated with a slit system to a size of 7 mm x 0.15 mm (horizontal x vertical) in order to allow a maximum footprint of the beam on the specimens at small incidence angles down to 0.1°, i.e. a full illumination of the specimens is already achieved at $\theta = 0.25°$. An additional cleaning slit with a vertical opening of 0.25 mm was used to reduce scattered radiation in the reflected beam detection. The 2D diffraction patterns were measured typically within about 60 s.

For analysis and interpretation of GIXRD 2D patterns one important aspect has to be kept in mind. All recorded GIXRD patterns only show a 2D angle segment so that the diffraction reflexes appear as an intersection of the diffraction cone with the detector surface in the case of a polycrystalline specimen with no preferred orientation [33]. Due to the distance between the specimen and the detector, the observed curvatures are generally weak, so that it is sufficient to integrate the intensity of the detector pixels perpendicular to the scattering plane in order to calculate a conventional diffraction profile from the 2D-data [33].

For the interpretation reference patterns for Fe, Cr, α-$Fe_2O_3$, γ-$Fe_2O_3$, $Fe_3O_4$, $Cr_2O_3$, α-$SiO_2$, β-$SiO_2$, $FeCr_2O_4$ and different carbides were calculated with PowderCell [34]. Furthermore, reference materials were also measured to get a correlation between detector channels and angles.

## 4 Results and Discussion

By different heat treatments the influence of process parameters to the surface morphology and especially to the friction behaviour was observed. In Tab. 1 the process parameters of eight realised heat treatments are shown. Process S4, S7 and S8 were performed with pure inert gas without monosilane addition to produce reference specimens. So it is possible to specify the impact of the $SiH_4$. The monosilane addition by the maintaining specimens was held between the first and the second stochiometrical points in the given ranges for the partial pressure of oxygen.

Tab. 1: Process parameters of the realised heat treatments

| specimen identifier | duration/ temperature | inert gas | partial pressure of oxygen in mbar |
|---|---|---|---|
| native (R1, R2) | - | - | - |
| treatment S1 | 60 min/500°C | $N_2 + SiH_4$ | $< 10^{-17}$ |
| treatment S2 | 120 min/480°C | $N_2 + SiH_4$ | $10^{-15} – 10^{-17}$ |
| treatment S3 | 30 min/500°C | $N_2 + SiH_4$ | $10^{-14} – 10^{-17}$ |
| treatment S4 | 30 min/500°C | $N_2$ | $(1.5 \pm 0.5)\ 10^{-1}$ |
| treatment S5 | 30 min/500°C | $N_2 + SiH_4$ | $10^{-13} – 10^{-17}$ |
| treatment S6 | 60 min/500°C | $N_2 + SiH_4$ | $10^{-15} – 10^{-17}$ |
| treatment S7 | 60 min/500°C | $N_2$ | $(1.5 \pm 0.5)\ 10^{-1}$ |
| treatment S8 | 60 min/500°C | Ar | $(1.5 \pm 0.5)\ 10^{-1}$ |

In a macroscopic inspection of the specimens already great distinctions are clearly visible resulting from the different heat treatments. In Fig. 4 macroscopic images of selective specimens illustrate these optical differences in general. Specimens which were treated in process atmospheres with very low partial pressure of oxygen like S1 always show no optical difference to native untreated specimens.

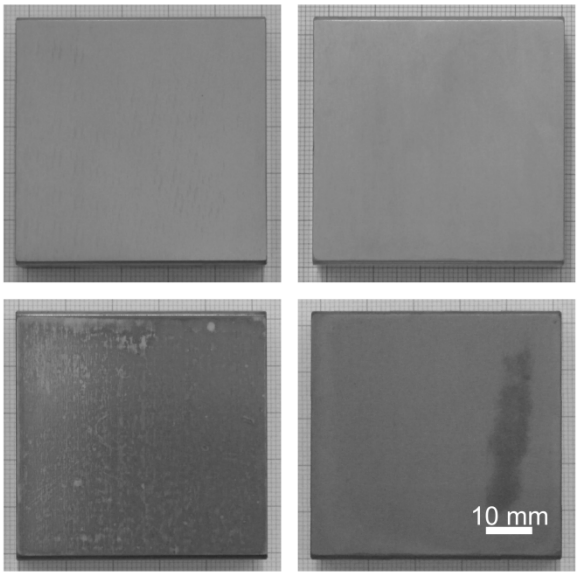


Fig. 4: Macroscopic photos of four specimens. Upper left: untreated native specimen R, upper right: specimen S1 after heat treatment, bottom left: specimen S3 after heat treatment, bottom right: specimen S4 after heat treatment

In contrast, specimens like S4 which were treated in pure inert gas and therefore at a high partial pressure of oxygen show in every case discolouration of the entire surface. Specimens treated in process atmospheres with a partial pressure of oxygen between $10^{-13}$ to $10^{-17}$ mbar show no uniform behaviour. Some of these specimens exhibit no significant changes while other exhibit dark discolourations like S3, which does not cover the surface entirely.

### 4.1 Strip drawing tests

In this chapter the results of the strip drawing tests are shown. Fig. 5 depicts the investigated friction coefficients for 10 specimens. Each bar shows the mean value of five reruns per specimen. Furthermore, for each bar an error indicator that represents the lowest and highest friction coefficient can be seen. The specimens S1 to S8 are selectively oxidised and thus coated with the new layer developed in the project. The specimens R1 and R2 are native references without coatings.

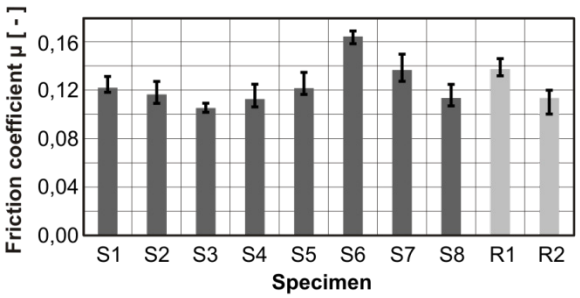


Fig. 5: Results of the strip drawing tests without deflection at a surface pressure of 18 N/mm²; Material of sheet metal strips DP600+Z, tool material 1.2379

The experiments with the specimen R1 were performed with cleaned sheet metals and without any lubrication. The second reference experiments with the specimen R2 were conducted with the use of deep drawing oil (WISURA AK 3080). The amount of the lubricant was with 2 g/m² equal to the amount which is required for simple drawing parts. The different selectively oxidised specimens (S1 to S8) are showing different results with regard to the friction coefficient. Overall, a clear trend to reduce the friction coefficient by the use of selectively oxidised surfaces can be observed. Especially the specimen S3 shows very promising results with approximately $\mu = 0{,}105$ and a small error indicator. The resulting friction coefficient of specimen S3 is even better than the result of the native oiled reference R2. In general the results of the specimens S1 to S8 should be compared with the native oil free reference R1, since this is a similar investigation with steel on steel.

### 4.2 SEM analyses

The strip drawing tests show that same specimen tested with no lubricant have comparable friction coefficient like the oiled reference and are clearly better than the reference specimen tested without lubricant. Now it is of great interest which surface modifications, especially crystallographic and morphology changes are responsible for this behaviour.

In Fig. 6 five SEM images which were made before the strip drawing test are shown. All treatments induce a change in the surface morphology even to the specimens which do not show optical differences on the macroscopic scale like S1, S5, S6. In contrast to the untreated

reference (R) here little particles on the surface can be detected now.

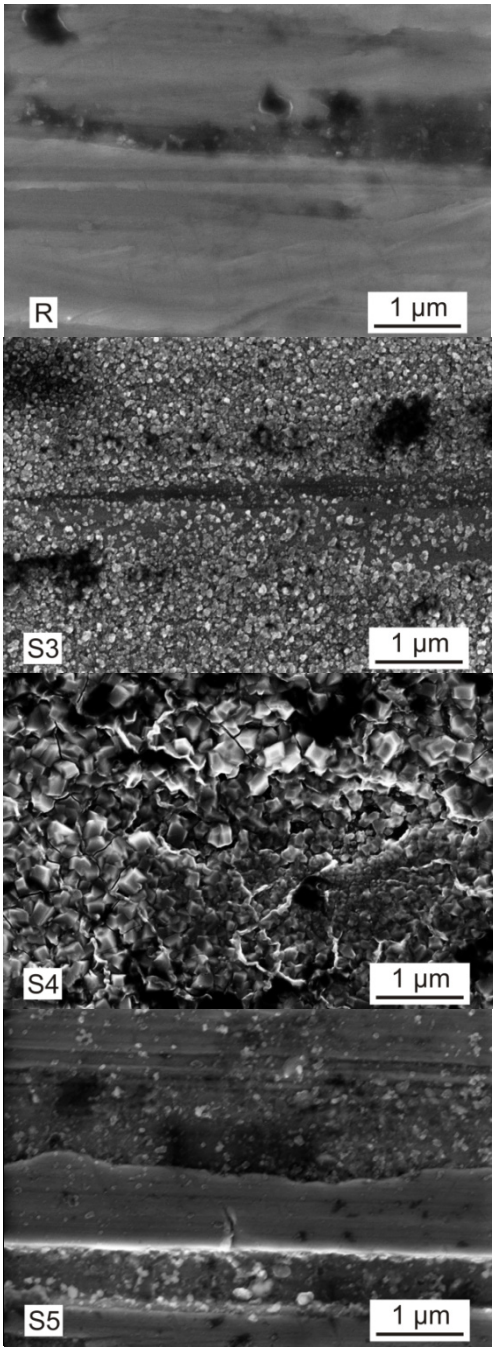


Fig. 6: SEM images. Top: untreated native specimen R, second from the top: specimen S3 after heat treatment, third from the top: specimen S4 after heat treatment, fourth from the top: specimen S5 after heat treatment

Specimens which were treated in pure inert gas show different behaviour (S4, S7 and S8). Here the entire surface is covered with comparable voluminous structures that becomes more voluminous for higher durations. The specimens with dark discolourations which were treated in an atmosphere with partial pressure of oxygen between $10^{-13}$ - $10^{17}$ mbar show a surface coverage of a tight carpet of small particles like S2 and S3. The SEM images indicate grain sizes of approximately 20 to 80 nm for the small particles.

### 4.3 GIXRD analyses

To get information about the chemical and crystallographic changes of the surface GIXRD patterns form the specimens at incident angle from θ = 1° up to 6° were collected. Fig. 7 depicts characteristic GIXRD patterns of different specimens (S2, R, S5, S3, S8 and S4) which were collected at an incident angle of θ = 2°.

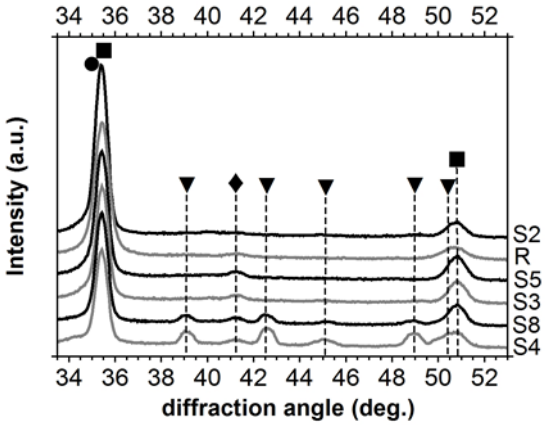


Fig. 7: GIXRD patterns of specimens S2, R, S5, S3, S8 and S4 at an incident angle of at θ = 2°. The reflexes are marked with symbols to indicate there origins. (α-Fe (■), Cr (●), α-$Fe_2O_3$ (▼), chromium-carbide compound (♦))

Every pattern has a mean reflex at about 35.4° that belongs to α-Fe (■) with a little shoulder on the left side that originates from Cr (●). A second reflex from α-Fe is located at about 50.7°. Specimens like S4 and S8 which were treated in pure inert gas as well as S7 show several α-$Fe_2O_3$ (▼) reflexes. This reflexes can be detected also for incident angle greater than θ = 5° that indicates a significant layer of α-$Fe_2O_3$ on the top of these specimens. Another reflex at about 41.5° (♦) can be detected for all specimens except S2 which is the only specimen which was treated at 480 °C instead of 500° C. As it becomes obvious this reflex becomes more dominant through the heat treatment independent of the process gas atmosphere. This reflex probably originates from a chromium carbide compound.

At an incident angle of 2° no more reflexes can be found. So the small particles on specimens S2 and S3 give no additional reflexes in comparison with native untreated specimens. This is an indication that the particles which form the adlayer are probably amorphous with an, at present time unknown, chemical composition. GIXRD patterns for smaller incident angles which will be more surface sensitive did not give proper diffractograms, because of the native roughness of the specimens. Furthermore the dispersion plays a key role [26, 27].

## 5 Conclusion and Outlook

The results of experiments show that the process parameters of the heat treatments have a great impact to the surface of the tool steel. The strip drawing tests and the SEM images suggest that a surface layer with a dence coverage of particles (S3) has the lowest friction coefficient. The friction coefficient is even smaller than the measured values for the uncoated lubricated refer-

ence R2. The grain size of the generated particles of S3 is well below 100 nm and the particles seem to be amorphous since no additional Bragg reflexes could be observed. The chemical composition of these particles is unclear so far and subject of actual investigations.

Specimens treated under pure inert gas have a better friction behavior then a uncoated non lubricated reference R1 as long the formed $\alpha$-$Fe_2O_3$ adlayer exhibit a dense structure like on S4 and S8. The archived friction coefficients of these two specimens are in the range of the lubricated reference R2.

In summary the results presented prove that the chosen approach to generate tool coating via a controlled oxidative heat treatment seems to be suitable to reduce the friction. This reduction is an essential requirement towards a dry metal forming process.

Towards a future application in a next step investigations concerning the wear resistance have to be performed.

## Acknowledgements

This work was financially supported by the DFG (reference numbers MA1175/41-1 and BE1690/170-1). The authors gratefully acknowledge the DELTA machine group for providing reliably synchrotron radiation. Particular, the authors appreciate the support of the company Tata Steel Europe Limited and gratefully thanks for the provision of the required sheet material.

## References

[1] Gesellschaft für Tribologie: Online resource of the “Gesellschaft für Tribologie”, www.gft-ev.de, (2015) last visit 24.01.15.

[2] H. Czichos, K.-H. Habig: Tribologie-Handbuch - Tribologie, Tribomaterialien, Tribotechnik, 3., überarbeitete und erweiterte Auflage, Viehweg + Teubner Verlag Wiesbaden (2010) 6.

[3] E. Doege, B.-A. Behrens: Handbuch Umformtechnik - Grundlagen, Technologien, Maschinen, Springer-Verlag Berlin Heidelberg (2007), 412-417, 808.

[4] S. Itasse: Umformen ohne Öl schützt die Umwelt, Vogel Business Media, maschinenmarkt.vogel.de, (2013).

[5] D. Schulz: Richtig angepasster Reinigungsprozess erhöht Qualität und Wirtschaftlichkeit, Vogel Business Media, maschinenmarkt.vogel.de, (2013).

[6] J. Kettner, S. Hübner, B.-A. Behrens: Zero Lubrication Forming of Pre-coated Sheet Metals, Proceedings of the 17th IFHTSE Congress 2008, October 27 - 30 in Kobe, Japan, Netsu Shori, Journal of the Japan Society for Heat Treatment, (2009), Vol. 49, Special Issue, Vol. 1, p. 213-216, ISSN 0288-0490.

[7] F. Vollertsen, F. Schmidt: Dry Metal Forming: Definition, Chances and Challenges. Int. J. Precision Engineering and Manufacturing – Green Technology 1/1 (2014) 59-62.

[8] Y.F. Gong, H.S. Kim, B.C. De Cooman: Formation of Surface and Subsurface Oxides during Ferritic, Intercritical and Austenitic Annealing of CMnSi TRIP Steel. ISIJ Int. 48 (2008) 1745-1751.

[9] F. H. Stott, C. Y. Shih: The influence of HCl on the oxidation of iron at elevated temperatures. Mater. Corros. 51 (2000) 277-286.

[10] M.A.E. Jepsona, R.L. Higginson: The influence of microstructure on the oxidation of duplex stainless steels in simulated propane combustion products at 1000 °C. Corros. Sci. 51 (2009) 588-594.

[11] R.Y. Chen, W.Y.D. Yuen: Review of the High-Temperature Oxidation of Iron and Carbon Steels in Air or Oxygen. Oxidation of Metals 59 (2003) 433- 468.

[12] A. Vesel, M. Mozetič, A. Zalar: Oxidation of AISI 304L stainless steel surface with atomic oxygen. Appl. Surf. Sci. 200 (2002) 94-103.

[13] J.O. Edstrom: The mechanism of reduction of iron oxides. J Iron Steel Inst 175 (1953) 289–304.

[14] V.B. Trindade, R. Borin, B.Z. Hanjari, S. Yang, U. Krupp, H. J. Christ: High-temperature oxidation of pure Fe and the ferritic steel 2.25Cr1Mo. Mat. Res. 8 (2005) 365-369.

[15] D. Lützenkirchen-Hecht, D. Wulff, R. Wagner, R. Frahm, U. Holländer, H.J. Maier: Thermal anti-oxidation treatment of CrNi-steels as studied by EXAFS in reflection mode: the influence of monosilane additions in the gas atmosphere of a continuous annealing furnace. J. Mater. Sci. 49 (2014) 5454-5461.

[16] J.S. Corneille, J.-W. He, D.W. Goodman: Preparation and characterization of ultra-thin iron oxide films on a Mo(100) surface. Surface Science 338 (1995) 211-224.

[17] I. Milosev, J.M. Abels, H.-H. Strehblow, B. Navinsek, M. Metikos-Hukovic: High temperature oxidation of thin CrN coatings deposited on steel. J. Vac. Sci. Technol. A 14 (1996) 2527-2534.

[18] J.M. Abels, H.-H. Strehblow: A surface analytical approach to the high temperature chlorination behaviour of Inconel 600 at 700°C. Corrosion Science 39 (1997) 115-132.

[19] E. Clauberg, C. Uebing, H.J. Grabke: Surface segregation on Fe 25%Cr 2%Ni 0.1%Sb single crystals. Surface Science 433–435 (1999) 617-621.

[20] E. Park, B. Hüning, M. Spiegel: Evolution of near-surface concentration profiles of Cr during annealing of Fe–15Cr polycrystalline alloy. Appl Surf Sci 249 (2005) 127-138.

[21] A.J. Davenport, M. Sansone, J.A. Bardwell, A.J. Aldykiewicz Jr., M. Taube, C.M. Vitus: In Situ Multielement XANES Study of Formation and Reduction of the Oxide Film on Stainless Steel. J Electrochem Soc 141 (1994) L6-L8.

[22] M.F. Toney, A.J. Davenport, L.J. Oblonsky, M.P. Ryan, C.M. Vitus: Atomic Structure of the Passive Oxide Film Formed on Iron. Phys Rev Lett 79 (1997) 4282-4285.

[23] G. Renaud: Oxide surfaces and metal/oxide interfaces studied by grazing incidence X-ray scattering. Surf Sci Rep 32 (1998) 5-90.

[24] L.G. Parratt: Surface Studies of Solids by Total Reflection of X-Rays. Phys Rev 95 (1954) 359-369.

[25] G. Lim, W. Parrish, C. Ortiz, M. Bellotto, M. Hart: Grazing incidence synchrotron x-ray diffraction method for analyzing thin films. J Mater Res 2 (1987) 471-477.

[26] M.F. Toney, S. Brennan: Structural depth profiling of iron oxide thin films using grazing incidence asymmetric Bragg x-ray diffraction. J. Appl. Phys. 65 (1989) 4763-4768.

[27] M.F. Toney, S. Brennan: Observation of the effect of refraction on X-rays diffracted in a grazing-incidence asymmetric Bragg geometry. Phys. Rev. B 39 (1989) 7963-7966.

[28] F.W. Bach, K. Möhwald, U. Holländer, C. Roxlau: SCIB - Self-Cleaning Inert-Gas Brazing - Ein neues Verfahren zum flussmittelfreien Hartlöten korrosionsbeständiger Konstruktionswerkstoffe, Tagungsband zum 8. Internationalen Kolloquium Hart- und Hochtemperaturlöten und Diffusionsschweißen (LÖT 2007, Aachen, 19. - 21. Juni 2007), DVS-Berichte, Nr. 243, S. 235-241. Düsseldorf: DVS-Verlag, 2007.

[29] M. Tolan, T. Weis, K. Wille, C. Westphal: DELTA: Synchrotron Light in Nordrhein-Westfalen. Synchrotron Rad News 16 (2003) 9-11.

[30] D. Lützenkirchen-Hecht, R. Wagner, S. Szillat, A. Hüsecken, K. Istomin, U. Pietsch, R. Frahm: The multi-purpose hard X-ray beamline BL10 at the DELTA storage ring. J. Synchrotron Radiat. 21 (2014) 819-826.

[31] C. Broennimann, E.F. Eikenberry, B. Henrich, R. Horisberger, G. Huelsen, E. Pohl, B. Schmitt, C. Schulze-Briese, M. Suzuki, T. Tomizaki, H. Toyokawa, A. Wagner: The PILATUS 1M detector. J. Synchrotron Radiat. 13 (2006) 120-130.

[32] P. Kraft, A. Bergamaschi, C. Broennimann, R. Dinapoli, E.F. Eikenberry, B. Henrich, I. Johnson, A. Mozzanica, C.M. Schlepütz, P.R. Willmott, B. Schmitt: Performance of single-photon-counting PILATUS detector. J. Synchrotron Radiat. 16 (2009) 368-375.

[33] B.B. He, U. Preckwinkel, K.L. Smith: Comparison between conventional and two-dimensional XRD. Adv. X-ray Analysis 46 (2003) 37-42.

[34] W. Kraus, G Nolze: POWDER CELL - a program for the representation and manipulation of crystal structures and calculation of the resulting X-ray powder patterns. J. Appl. Crystallogr. 29 (1996) 301-303.